6. STAR MAPPER DATA PROCESSING

The star mapper data formed the second data stream for the Hipparcos satellite. Its primary goal was the provision of measurements for monitoring the attitude of the satellite, using the transits of selected stars through two sets of four slits. The recognition of transits and determination of transit times and signal intensities is the subject of this chapter. The continuous data stream from the same detectors was analysed as the Tycho data stream, of which the processing is described in Volume 4.

6.1. The Measurement Principles

The Star Mapper Slits

Star mapper slits were situated on either side of the main grid, but only those preceding the main grid in the scanning motion were used during the mission. There were two slit groups, 4 inclined slits, followed by 4 vertical slits (as shown in Figures 6.1 and 6.2). The uneven spacing of the slits made it possible to recognise a transit in absolute sense (contrary to the regular main grid, where the transit time had an ambiguity of an integer number of slit-intervals). The average width of each slit was 0.909 arcsec in the vertical slit-group, 0.916 arcsec in the inclined slit-group upper branch, and 0.922 arcsec in the lower branch. The variations in width were less than 0.1 per cent.

The star mapper signal was acquired from all information coming through the entire grid. Thus, it mixed data from different parts of the sky, both due to the superposition of the two fields of view as well as due to the size of the area covered. The signal was split into a B and V channel, roughly equivalent to B_J and V_J channels, and referred to as B_T and V_T, the T standing for 'Tycho' (see also Volume 1, Section 1.3).

The Data Sampling and Extraction

The data were sampled at a rate of 600 Hz simultaneously in the two channels. At the nominal scanning rate of 168.75 arcsec s^{-1}, the grid line spacings corresponded to intervals of 40, 60 and 20 sampling periods. The extraction of samples for processing by NDAC and FAST was based on the real-time attitude determination and the apparent positions of the stars at the time of observation. This predicted transit time as well as the star identifier formed part of the star mapper record.

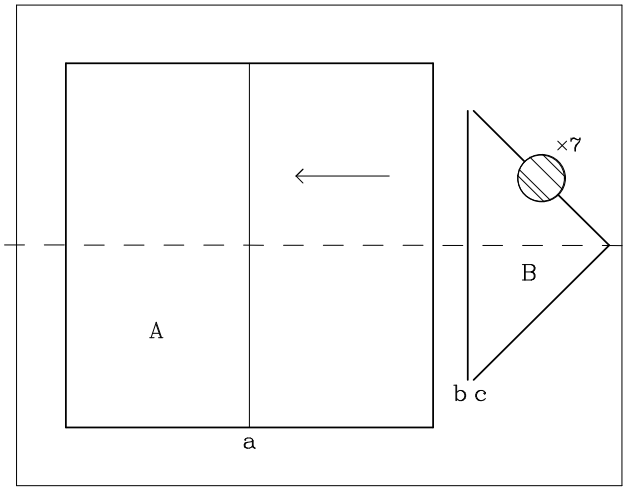

Figure 6.1. *The star mapper slits (B) relative to the main grid (A). The scan direction, i.e. the motion of a star, is indicated by the arrow. The fiducial reference line for the main grid is indicated by 'a', for the vertical slits by 'b' and for the inclined slits by 'c'.*

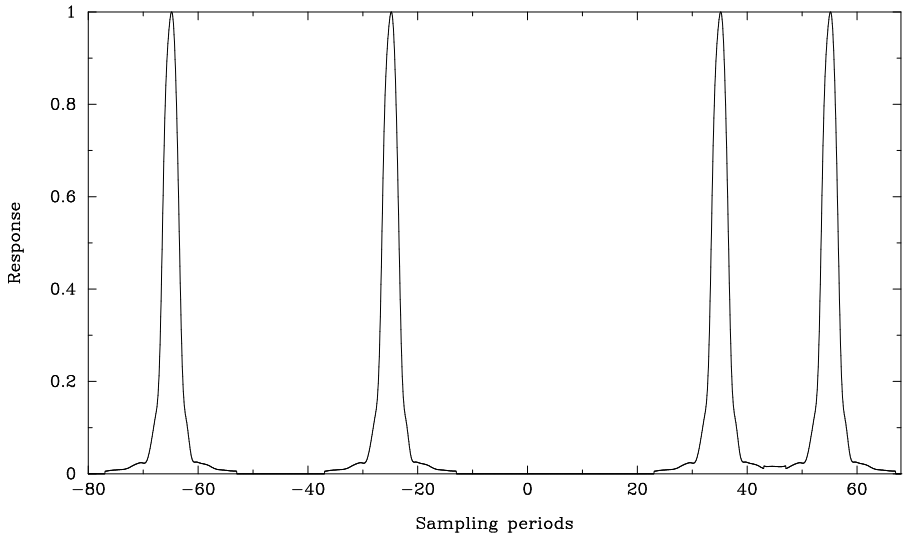

Figure 6.2. *The reconstructed slit response for a transit through the vertical slits in the preceding field of view. The detector is the V_T channel. The origin on the horizontal axis corresponds to the fiducial reference line.*

In the telemetry, samples were grouped in batches of 25, and 10 of these groups were extracted at ESOC for every star mapper transit record. In the NDAC processing, information from all 250 samples was used to optimise the detection of possible parasitic transits, and for the processing of double stars. This could also improve the distinction of data that could be associated with background measurements. In the FAST processing 200 samples were extracted based on the predicted transit time, from 91 samples before to 108 samples after the sampling closest to this transit time. Stars fainter than magnitude $B \simeq 10$ mag were not included in this selection.

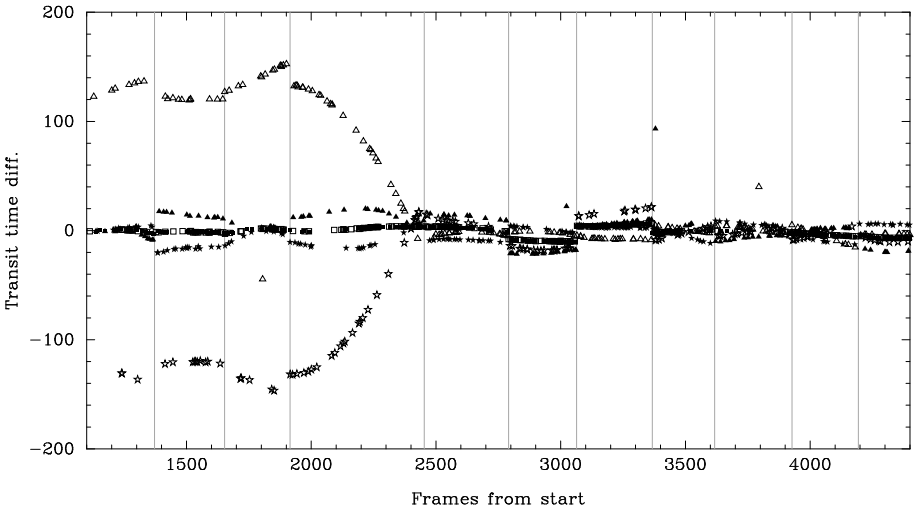

Figure 6.3. *The differences in 600 Hz sampling periods, between observed transit times and real-time attitude based predictions, showing the convergence of only one field of view at the start, followed by both fields of view from frame 2400 onwards. Transits through the vertical slits are indicated by squares, for the inclined slits by triangles for the upper branch, and stars for the lower branch. Filled symbols refer to the preceding field of view, open symbols to the following field of view. Thruster firings are indicated by the dotted lines.*

The use of the real-time attitude determination in the extraction process meant that when the on-board attitude had not converged, the extracted photon counts could entirely miss the stellar transit signal. The detection of the star mapper transits in the provided extracts, and the comparison between the predicted transit time and the transit time observed was therefore a powerful means of checking the performance of the real-time attitude reconstruction at any time. In NDAC, graphs were made of these differences for all data received, and time-intervals with bad attitude convergence thus recognised were excluded from further reductions. The FAST consortium relied primarily on the quality flag provided by ESOC for this purpose (see Section 5.1) which was in the first year of the mission not able to recognise the convergence of one field of view from the convergence of both fields of view. In this case transits went undetected in at least one field of view. Obviously in such instances the involved transits between two consecutive thruster firings were rejected by the attitude processing, the attitude was not computed and no image dissector tube transits were processed. In addition an *a posteriori* comparison of the grid abscissae computed on ground with the pointing derived from the coil current (on-board computation) allowed poor pointing due to either bad attitude or wrong celestial coordinates of the star to be detected and these transits were removed from the photometric solution. Figure 6.3 shows an extract of a monitor plot made by NDAC.

The average time interval between star mapper transits extracted for the attitude reconstruction was set by the density of these stars on the sky ($\simeq$ 2 deg^{-2}), the span of the star mapper slits (0.667 deg) and the scan velocity of the satellite, 0.0469 deg per second. This gave per slit group and per field of view on average one transit every 16 s. The total data-stream thus consisted of approximately one transit every 4 s. This number could vary by 20 to 30 per cent depending on the inclination of the scanning circle with respect to the galactic plane. The total sky area as seen by the star mapper slits was 0.025 deg^2. Down to about 10 mag, with close to 10 stars per square degree, an average of 10 per cent of all transits were at least double. This number varied considerably with

galactic latitude. Considering all possible transits that could be detected, originating from about 1 million stars over the entire sky, the chances of getting a completely clean transit were rapidly diminishing. However, most of the disturbing transits were too faint to cause serious problems.

The Single-Slit Response Functions

The single-slit response functions represented the normalised intensity profiles caused by a stellar image passing across a single slit at nominal scan velocity, integrated over sampling periods of 1/600 s. The profiles were different for the two slit groups, and in the case of the inclined slits, also for the upper and lower branch. They were also different for the two fields of view and for the two photometric channels. The response functions were obtained from selected transits of brighter, single stars (between magnitudes 4 and 8). Initially, at the start of the mission, data had to be reduced with pre-launch estimated response functions. From this data the first calibrated response functions were obtained. In NDAC, the final reductions were all done with a final set of evolving response functions, based on data accumulated over intervals of 2 to 3 months.

As stated above, the calibration of the response functions used data from transits of relatively bright stars. These transits, through all four slits, had been assigned a reference transit time and a relative scan velocity (see Section 6.3). The positions of the four slits as projected on the sky were known from the calibration described below. The background signal had been derived in the data reduction (see Section 6.3 and 6.4). The measured intensities, after subtracting the background signal, were assigned to bins according to their distances from the assumed slit centre. Where the wings of the intensity profiles overlapped, data were not used. Data were first accumulated for individual slits at different positions along the slits, and then added for the four slits for the different positions along the slits. Data from 30 000 to 40 000 transits were used per calibration, describing the response functions at a time resolution of 9600 Hz (i.e. 16-fold oversampling) with some 2000 contributing data points per bin. The wings were only followed to 4 arcsec from the centre of the slit, but it was clear from data for very bright stars that the wings extended well beyond this range, albeit at a low level (see also Volume 4, Section 4.2 and Figure 4.3).

The averaged data per bin were fitted with a spline function, which was subsequently rescaled to give a maximum response of 1.0. The spline functions also provided the derivatives of the response functions, which was essential for transit time estimates. The fitted response functions are in the following represented by $R_q(t - t_0)$, where t_0 is the transit time at the designated slit centre, taken to be the point halfway between $R_q = 0.5$ on the rising and descending branches of the single-slit profile. The index q represents one of the 16 different combinations of slit group, upper/lower branch, passband and field of view. Examples of two fitted response functions and their derivatives are shown in Figure 6.4.

The procedure described above was as applied by NDAC. The FAST procedure followed the same general principles, but differed in the following respects:

(1) in selecting the transits, only photometric standard stars were retained for normalisation. In order to avoid contamination by double or parasitic stars, all transits which showed a large deviation from the expected brightness, or failed any of the statistical tests described in Section 6.5, were rejected;

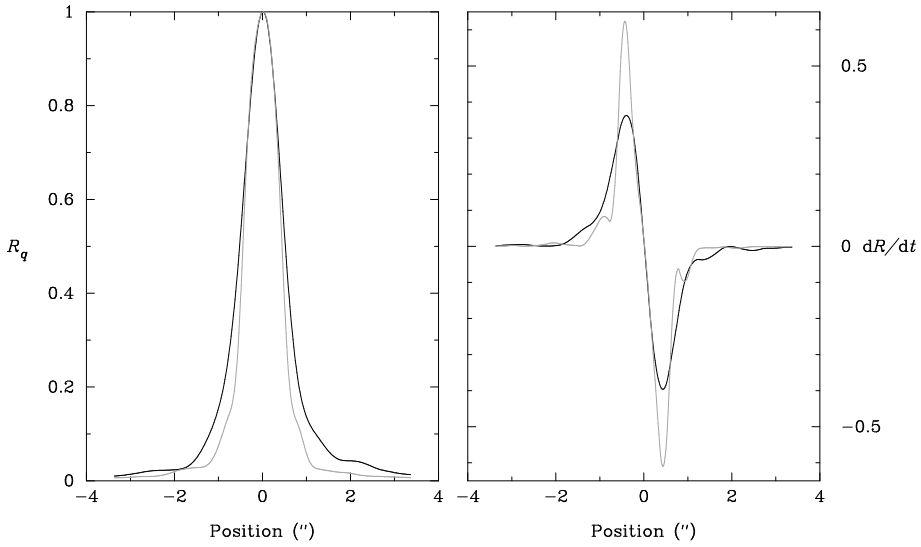

Figure 6.4. *The single-slit response functions (left) and their derivatives (right) for the inclined slits (solid line) and vertical slits (dotted line), upper branch, in the preceding field of view, recorded in the B_T channel. The derivative is given as change of response per 600 Hz sampling period. At nominal scan-velocity, one sampling period corresponds to 0.28 arcsec.*

Table 6.1. Calibrated distances between star mapper vertical slits compared with the ground calibration values.

Interval	arcsec	mm	ground (mm)
1 to 2	11.247	0.07638	0.07640
2 to 3	16.867	0.11455	0.11460
3 to 4	5.623	0.03819	0.03820

(2) the time resolution of the response function was 1/32 arcsec (5400 Hz) and the table extended to ±2.3 arcsec (half of the smallest slit distance);

(3) the centre point was determined as in NDAC, but R_q was normalised to unity at the centre point, leading to values slightly above 1.0 at the maximum for asymmetric cases (1.005 maximum).

Some evolution of the response functions took place during the mission, possibly associated with the overall temperature of the spacecraft. There were no significant differences found for stars of different colour index, although this could not be checked for very red stars because of insufficient data.

Calibration of the Slit Spacings

The spacings of the slits were calibrated from cross-correlations between the data collected for the individual slits. This showed the offset of the actual centres of the four slits from the assumed centres. The response functions for the four slits were effectively identical. Separate calibrations were obtained for the vertical slits and the upper and lower branches of the inclined slits. The calibrated separations are shown for the vertical slits in Table 6.1. In both consortia, individual slit distances were obtained for all cases mentioned above.

Similarly, the position of the inclined slits with respect to the vertical slits had to be calibrated. In NDAC this was done as an optional part of the attitude reconstruction software, which allowed also for the calibration of the slit orientations. In FAST, a full calibration was performed as described in the following sections.

Medium-Scale Distortion Corrections

The star mapper slits were created through engraving transparent lines in a non-transparent layer deposited on a piece of glass, which was spherically convex to match the focal plane curvature. The engraving was made in small areas, referred to as scan-fields. After the production of the grids they were measured for irregularities. This produced the medium-scale distortion values, which together with the slit orientations and relative positions provided a clean reference frame to which star mapper transit times could be referred. In NDAC, the implementation of the medium scale distortions (being not entirely unambiguous in direction and orientation) was checked using accumulated residual transit times for star mapper transits, obtained after reconstruction of the satellite attitude. The medium scale distortions were of the order of 0.01 arcsec, with a maximum of 0.05 arcsec.

In FAST, the slit distortion, that is the difference between the theoretical positions of the mean slits and their actual positions as projected on the sky (including consequently the grid-to-field transformation) was split into two components:

(1) a slope with respect to the ideal orientation (vertical or at 45° inclination). This was essentially due to the rotation of the grid with respect to its ideal position. This linear slit model imposed a fixed intersection with the horizontal axis at the following abscissae from the centre of the grid:

$$G_v = -0.009\,370\,100$$

for the vertical slit, and:

$$G_i = -0.015\,443\,305$$

for both inclined slits, the unit being grid radians;

(2) a shift ΔG with respect to the linear slit model along the horizontal direction was defined for the 34 equal scan-fields dividing each half-grid.

During the first year of data reduction, the slope was deduced from the global grid rotation determined by the great-circle reduction software run by the ‘First Look’ task (see Chapter 4 and Volume 2, Section 9.2), while ΔG was taken from the measurements made on the ground, the grid-to-field transformation being assumed known. Later, a direct calibration of the slit distortion was performed.

FAST Slit Distortion Calibration

From the great-circle reduction task (Chapter 9), the following results were obtained and used for the star mapper grid calibration:

- the smoothed along-scan attitude with an accuracy of the order of a few milliarcsec, this then gave the scan velocity to significantly better than 1 mas per frame period ($T_4 = 2.133\ldots$ s), except around thruster actuations;
- mean abscissae of stars to within a few milliarcsec accuracy in the same reference frame.

In addition, improved star positions were available for most single stars from the preliminary sphere solution so that, in the same reference frame, one could compute the apparent coordinates of the star to a precision of a few milliarcsec in both coordinates. The main uncertainty thus came from the star coordinates.

The next step was to determine the theoretical transit times on the ideal grid, using the known attitude and star coordinates. The differences with the observed transit times were transformed into the shifts ΔG. This quantity was stored together with the perpendicular grid coordinate H of the star (Section 5.4) and the slit index q. Only 'safe' data were kept: all observations made within $\pm 4T_4$ of a thruster firing were rejected, as were stars known or suspected to be double, or having unknown magnitudes or inaccurate positions and observations presenting a large ΔG. Each reference great-circle set provided some 2000 to 4000 data points.

Twenty data sets were chosen from among the best in each calibration period of about one month (see Chapter 4). These $\simeq$ 50 000 data points were used to compute by linear regression the slope of each half-grid system. Then, the residuals of this regression were used to compute, for each scan-field, the medium-scale distortion. The resulting precision was about 0.5 arcsec to 1 arcsec for the slopes and, for ΔG, 5 mas on the vertical slits and 10 to 18 mas on the inclined slits. This precision was more than sufficient for the needs of attitude reconstruction. The calibration also provided the separation between the star mapper slit system and the main grid.

6.2. The Star Mapper Transit Signal

The star mapper photon counts N_k, collected at time t_k by either channel $c = B_T, V_T$ during the passage of a star, were described as a sequence of statistically independent and Poisson-distributed counts, having the following time-varying average:

$$\mathrm{E}[N_{k,c}] \equiv I_{k,c} = I_{b,c} + I_{s,c} \sum_{j=1}^{4} R_q(t_k - \tau_j) \qquad [6.1]$$

where $I_{b,c}$ and $I_{s,c}$ are the intensities of the background and star, respectively, R_q is the single-slit response function, and τ_j are the transit times at the four slits. Given R_q and the observed counts, this model could be fitted to give the background and star intensities and the four slit transit times. The transit time of the whole slit group was then defined as the unweighted mean value, $\tau = \langle \tau_j \rangle$. However, this procedure would only work if all four slit transits were available. Moreover, it does not take advantage of the very precise knowledge of the slit spacings available from the calibrations. An alternative method was therefore needed which incorporated the calibrated slit spacings.

Evidently the time τ corresponds to the transit of the star image across an imaginary line situated at the mean coordinate, in the scan direction, of the four slit centres; this defines the 'fiducial reference line' of the slit group (Figure 6.2). Let d_j be the calibrated positions of the slit centres from this line, such that $\sum_j d_j = 0$. Provided that the local scan velocity v_q is known from the attitude reconstruction, the slit transit times can then be referred back to the fiducial line by means the formula $\tau = \tau_j - d_j / v_q$, and the group transit time can be obtained also from an incomplete transit. Alternatively, if $\tau_j = \tau + d_j / v_q$ is substituted into Equation 6.1, the whole group transit may be fitted with only the three parameters $I_{b,c}$, $I_{s,c}$ and τ.

The calibration of the position of the fiducial reference line with respect to the main grid by FAST is described in the preceding section. In NDAC, it was obtained from a feed-back of calibration results from the great-circle reduction, which accurately related star mapper based reconstructed attitude to the fiducial reference line on the main grid (see Chapters 5, 9 and 10).

Scan Velocity

In the FAST solution, the four values τ_j were estimated, and from their mean value τ was derived. As long as all four values were available, this made the transit time determination independent of the scan-velocity derivation. When only three values were available, the scan velocity based on the real-time attitude determination was used, which even under worst conditions introduced an error less than 20 mas, negligible with respect to the requirements.

In the NDAC solution, the scan velocity was derived using gyro data (see Chapter 7), which reduced the solution to an estimate of only one transit time parameter, τ. The scan velocity had to be known for each field of view along, and perpendicular to, the scan-direction. Variations with respect to the nominal scan-velocity amounted to a maximum of 3 to 4 arcsec s^{-1}, a few per cent of the nominal scan velocity of 168.75 arcsec s^{-1}. The main effect of the variations in scan-velocity was on the spacing of the slit transits in time. The effect on the width of the response function was very small.

At a minimum accuracy of 0.05 arcsec s^{-1} for the gyro-based scan velocities, the maximum error on the slit spacing for the first and last slits was of the order of 0.002 arcsec, giving maximum response estimate errors of 0.2 per cent, which were only relevant at intensity levels where the photon counts were already affected by the much more damaging effects of saturation. The accuracies obtained for the scan velocities from the gyro data were therefore in normal conditions more than sufficient for the star mapper signal processing. At times of gyro breakdown this was not always the case, and provisions could have been, but were not, made to correct scan velocities for the very brightest objects.

The effective spacings of the inclined slits were in addition affected by the rotation of the grid by $\simeq 5$ arcmin. For the lower branch they became wider by 0.17 per cent, for the upper branch narrower by the same margin. This was accommodated in the calibrated slit spacings.

6.3. Signal Recognition and Background Determination by NDAC

The star mapper counts had to be searched for the presence of one or more transit signals. For this purpose, the counts from the B_T and V_T channel were added, and combined in pairs, so that the resulting signal contained 125 samples at 300 Hz. A provisional background was subtracted from this signal to leave primarily counts related to star transits:

$$J(k/2) = \sum_{c=B_T,V_T} \left(I_{k-1,c} + I_{k,c} - 2\bar{I}_{b,c}\right), \quad k = 2, 4, 6 \ldots 250 \qquad [6.2]$$

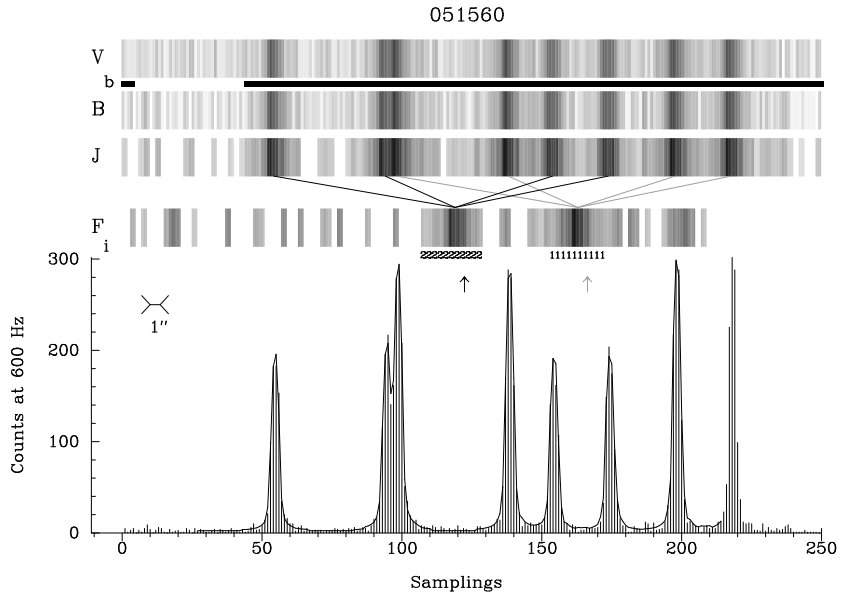

Figure 6.5. *NDAC processing of star mapper data for a transit of the double star HIP 51560/51561 through the vertical slits. The first two bars show the original counts, the third bar the cumulated signal J, and the fourth bar the filtered signal F. Between the V_T and B_T signals is indicated which samples were excluded from the calculation of the background (all samples coinciding with the black line at b). Below F are indicated the recognised transits: here the programme star transit is fainter than the companion. The arrows below indicate the predicted positions (as based on the real-time attitude determination). The lower half of the graph shows the original B-channel counts folded with the final signal fit. This fit was not made for the first 26 and last 35 samples, as undetected single transit peaks could occur there.*

All negative values of $J(k/2)$ (counts below the estimated background level) were reset to zero. This signal was subjected to a multiplicative filter. This filter consisted of four Dirac functions, spaced like the expected slit responses. With a time resolution of 300 Hz no corrections for scan-velocity variations were needed, and the spacings were fixed at 20, 30 and 10 intervals:

$$F(l) = \left[\prod_n J(l+n)\right]^{1/4}, \quad n = -30, -10, 20, 30 \qquad [6.3]$$

When $l - 30$ or $l + 30$ was outside the range covered by J, only three inputs were considered; when two values were outside the range, only the remaining two were used. Single peaks close to the start or the end of the 250 samples could not be detected. Such samples were also *a priori* excluded from background calculations. This reduced the signal of every star transit to one peak. An actual signal could be recognised as a cluster of $F(l)$ values different from zero. When more than one transit was present, then each transit produced its own cluster. Due to the cumulation of the data before filtering it was possible to recognise still relatively faint signals, and under normal conditions (background typically 2 to 4 counts per sample of 1/600 s), there was no difficulty in recognizing the faintest programme stars in the star mapper data stream, $\simeq$ 10 mag. Figure 6.5 shows an example of the various stages in the recognition and processing.

The individual clusters in $F(l)$ provided first estimates of τ (as in Equation 6.1) associated with these possible transits. A special mechanism, similar to that used in

automated star counts from plate scans, was designed to separate almost overlapping peaks. Depending on the magnitude differences, separations down to 1.5 arcsec could still be handled in the reductions. Similarly, up to three additional transit signals could be present without losing the programme star signal. In such a case, the signal most closely resembling the magnitude and colour of the programme star was identified as the programme star, or, if this were ambiguous, the transit closest to the expected transit time.

When known double stars were encountered, a prediction of the expected separation of the transit signals was made, against which the observed signals were matched. This allowed star mapper processing of some 1200 Hipparcos double stars with separations more than 1.5 arcsec, resulting often in much improved coordinates, and occasionally improved separations and orientations.

Background Determination

The estimates of τ, together with the slit spacings, defined where single-slit transit signals could be expected in the original samples, and conversely, which samples were most likely to represent only a background signal. The mean and standard deviation of these background samples were determined, and checked for outliers due to spikes. When, after four iterations, the observed standard deviation was still more than 1.25 times the expected standard deviation (assuming the background counts represented a stochastic Poisson process, the expected standard deviation was equal to the square root of the mean count observed), then the background was rejected and replaced by the estimated background obtained from a running mean of earlier star mapper background determinations. This running mean consisted of the mean of the last successfully measured background and (up to) 9 times the previous running mean. The running mean was also used as first background estimate in the filtering described above (Equation 6.2).

Background data were accumulated independent of whether a signal was detected or not. Levels of background varied considerably, primarily due to the sensitivity of the star mapper detectors to high energy radiation from outside the satellite. The star mapper background has provided a 3.5 year record of the radiation activity inside and outside the van Allen belts during a period of high solar activity. Away from the radiation environment, background levels varied between 1200 and 3600 Hz, or 2 to 6 counts per sample interval of 1/600 s. During van Allen belt passages, however, it could increase to several hundred counts per sample, and at times of high solar activity to well over 1000 counts and occasionally to complete saturation (see also Figure 2.2).

6.4. Signal Recognition and Background Determination by FAST

Efficient estimates could be provided by the maximum likelihood principle, if all star mapper samples N_{k,B_T} and N_{k,V_T} were the realization of a Poisson stochastic process with the average as defined in Equation 6.1, i.e. a superposition of a background signal and the four peaks of the programme star signal. Owing to parasitic transits and overlapping programme star transits, as well as to spikes in the data, this was in general not true for all photon counts in a record. A detection procedure was therefore implemented to extract the sequence $\mathcal{C}$ of model-consistent samples. Then the model parameters could

be estimated by maximizing the logarithm of the likelihood function, restricted to the model-consistent samples:

$$\ln L(\tau_1, \tau_2, \tau_3, \tau_4, I_{b,B}, I_{b,V}, I_{s,B}, I_{s,V}) = \sum_{c=B_T,V_T} \sum_{k\in\mathcal{C}} \left[N_{k,c} \ln I_{k,c} - I_{k,c} - \ln(N_{k,c}!)\right] \qquad [6.4]$$

Moreover, since the four slit transit times τ_j were sufficient statistics for the transit time τ, they in turn provided an efficient estimate for τ.

To extract the model-consistent sequence $\mathcal{C}$ the detection process had to separate the star mapper record into three subsets of samples:

(1) the background samples, i.e. samples consistent with the hypothesis H_b: $I_{k,c} = I_{b,c}$ of a constant intensity;

(3) the (single) star samples, i.e. samples consistent with the composite hypothesis H_s: $I_{k,c} = I_{b,c} + I_{s,c} \sum_{j=1}^{4} R_q(t_k - \tau_j)$;

(3) the samples biased by parasitic or overlapping stars, i.e. samples not consistent with any of the above models (composite hypothesis H_p).

All the different tests applied to a generic sample m to discriminate among the above hypothesis were based on five variables $T_j(m)$, $j = 0, 1 \ldots 4$, obtained from the convolution of the cumulated counts of the B_T and V_T channels with the single-slit response function:

$$T_j(m) = \sum_{c=B_T,V_T} \sum_{k} N_{k,c} R_q(t_k - t_m - d_j/v_q) \qquad [6.5]$$

where t_m is the mean time of the sample m, and $d_0 = 0$. Figure 6.6 shows a record of photon counts for a 6.6 mag programme star, and the corresponding convolution $T_0(m)$. By comparing the convolution with a suitable threshold s, the value of which depended on the hypothesis that had to be verified, the boolean test variables $L_j(m)$ were obtained: $L_j(m) = 0$ if $T_j < s$, $L_j(m) = 1$ otherwise (see Figure 6.7).

The convolution and channel cumulation allowed the effect of photon noise on the tests to be reduced. It should also be noted that, under Poisson statistics, the convolution $T_j(m)$ tends to the log-likelihood ratio as $I_s/I_b \to 0$, and it yields a good approximation when $I_s/I_b \simeq 1$, i.e. when the star intensity is comparable to the background. This case represented the most critical situation for separating purely background samples from star-biased samples since, for the faintest programme stars included in the star mapper data stream ($\simeq$ 10 mag), the star intensity was normally of the same order as the background.

The further processing of the star mapper data was partitioned into three main steps:

(1) detection of background samples and background determination;

(2) detection of programme star samples (if any); when a single star could be detected, a first estimate of the four slit transit times and the star intensity was obtained;

(3) maximum likelihood estimation of the transit time and of the star intensity for both channels.

Item (1) is described hereafter, while (2) and (3) are covered, respectively, in Sections 6.5 and 6.7.

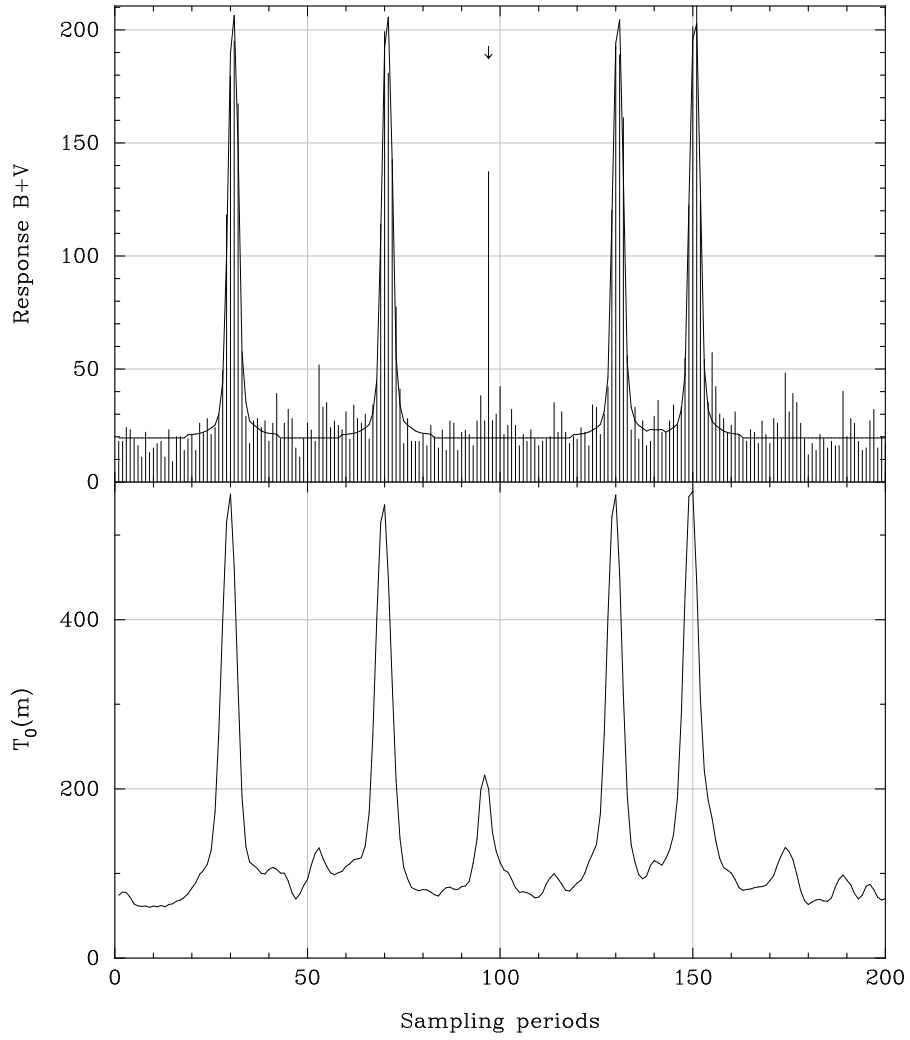

Figure 6.6. *Top: a photon count record of a 6.6 mag star (HIP 47115) through the vertical slit-group, with the estimated average signal superimposed. The abscissae are in sample units (1/600 s), the ordinates in counts per sample. A spike, which occurred in the V_T channel, is indicated by an arrow. Bottom: the corresponding convolution $T_0(m)$.*

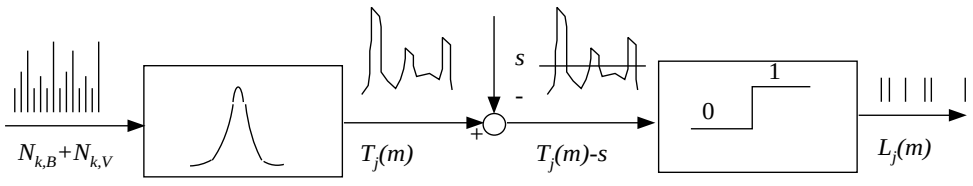

Figure 6.7. *A sketch of the construction of the basic test variables.*

Background Detection and Estimation

Background estimation for both channels was made independently from subsequent processing (star intensities and transit time determinations). The background in the star mapper signal was defined as a Poisson-like stochastic process having constant average for a single transit but variable from one transit to another: the sky background was variable and the photomultipliers were sensitive to the radiation environment (van Allen belts). The background detection process compared two alternative hypothesis: the null-hypothesis H_b (constant background) and the alternative hypothesis $H_s \cup H_p$ (programme or parasitic star signal).

A generic sample m was accepted as a background sample if $L_0(m) = 0$ and $|m - n| > n_0$ for all n such that $L_0(n) = 1$. The first condition, $L_0(m) = 0$, occurring when $T_0(m) < s_0$, detected the samples acceptable as background samples. The second condition, depending on the integer threshold n_0, rejected in addition those which were likely to be biased by star signals. This refinement of the detection process aimed at reducing as far as possible the risk of attributing a star-biased sample to background and avoid its overestimation. The expression of the significance threshold s_0 was the following:

$$s_0 = \bar{T}_0 + 2.3S_0 \qquad [6.6]$$

where $\bar{T}_0 = \bar{I}_b \int R_q(t)\mathrm{d}t$ was the average and $S_0^2 = \bar{I}_b \int R_q^2(t)\mathrm{d}t$ the variance of the convolution $T_0(m)$ under hypothesis H_b. Here, $\bar{I}_b$ designates the running background estimate explained below. The numerical factor 2.3 was set by fixing the risk of rejecting a background sample. The risk was fixed to a value not particularly low, about 1 per cent, since the major concern was to minimise the risk of attributing a star-biased sample to background. This risk was further reduced by removing the background samples biased by a star transit signal. Accepting such samples as background samples would otherwise have resulted in an overestimation of the average background, with the risk of not detecting faint programme stars in subsequent processing. The background samples detected in a record were then averaged to produce the (local) background estimates for the transit:

$$\hat{I}_{b,V_T} = \frac{1}{n}\sum_{k\in\mathcal{A}} N_{k,V_T}, \qquad \hat{I}_{b,B_T} = \frac{1}{n}\sum_{k\in\mathcal{A}} N_{k,B_T} \qquad [6.7]$$

where n is the number of accepted background samples and $\mathcal{A}$ is their sequence in the record.

Since the detection test assumed known background statistics, a running estimate of the background, $\bar{I}_b$, was maintained during the whole data set (between 5 and 8 hours). This allowed the risk of rejecting background samples as described above to be increased, without hampering the precision of background estimates as based on the samples from successive and semi-contiguous records.

The running estimates were updated at each transit i from the local estimates $\hat{I}_{b,B_T}(i)$ and $\hat{I}_{b,V_T}(i)$. A first-order Kalman filter was used for each channel:

$$\bar{I}_{b,c}(i) = [1 - K(i)]\bar{I}_{b,c}(i-1) + K(i)\hat{I}_{b,c}(i) \qquad [6.8]$$

where the time varying gain was set to $K(i) = n(i)/(n(i)+250)$, depending on the number $n(i)$ of detected background samples, but restricted to the range $0.05 \le K(i) \le 0.5$. This range was designed to trade off between two contrasting goals: attenuating the photon

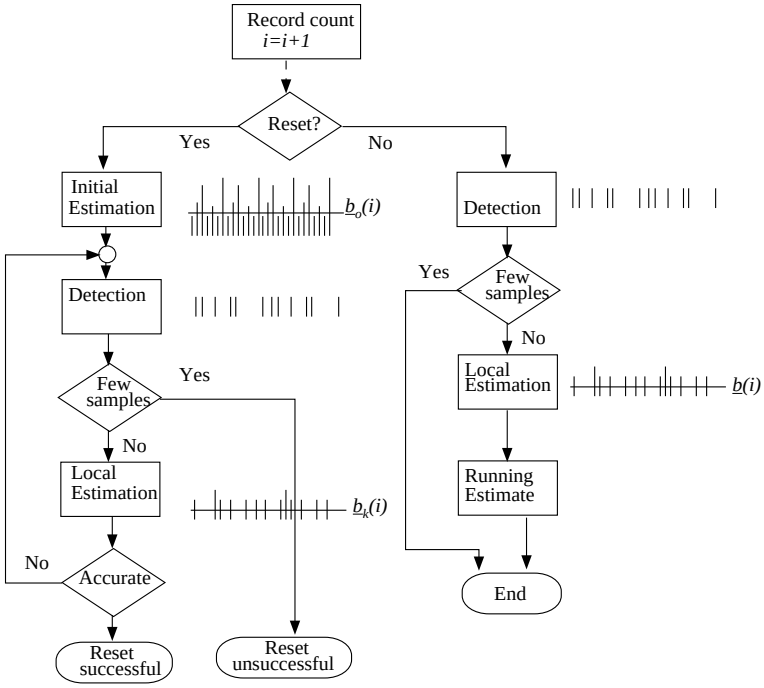

Figure 6.8. *Flow chart of the background detection and estimation.*

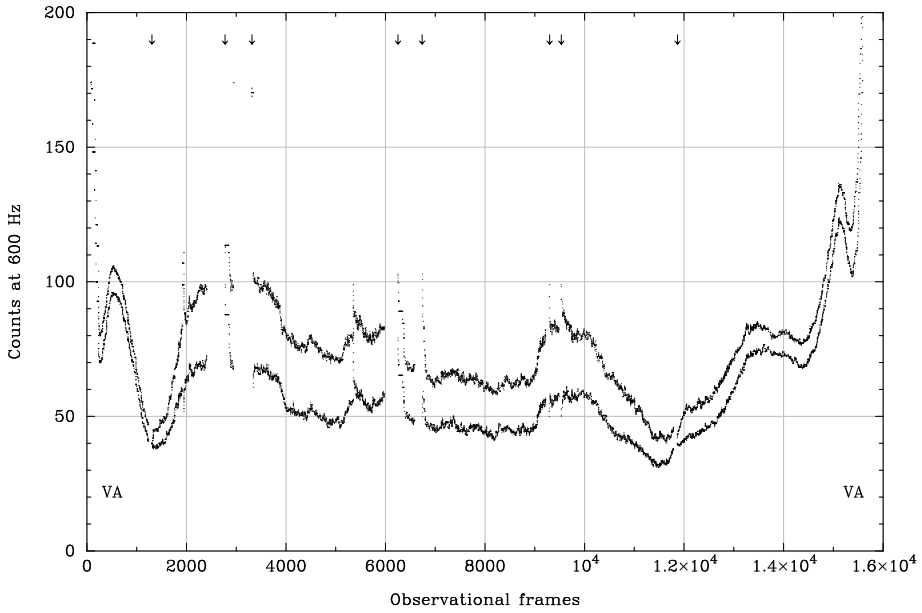

Figure 6.9. *The estimated background intensity over an orbit on 10 June 1991, coinciding with a period of very high solar activity. The background levels detected at apogee (centre of the graph) were one order of magnitude higher than under normal conditions. The top curve represents the V_T channel, the lower curve the B_T channel. The van Allen belt crossings are indicated by VA, resets of the Kalman filter by arrows.*

noise error (typically when the background was low and few samples could be detected), and tracking the real background variations. The processes described above are also shown in a flow diagram in Figure 6.8. An example of the running background estimate for a time interval with particularly strong background variations is shown in Figure 6.9.

Under normal conditions, i.e. when the running estimate $\bar{I}_b = \bar{I}_{b,V_T} + \bar{I}_{b,B_T}$ of the total background was assumed to be accurate and reliable, the significance threshold s_0 of the detection test was computed as a function of $\bar{I}_b$ according to Equation 6.6. When the running estimate was likely to have lost accuracy, e.g. after a large interruption in the observations (more than 1 minute), it had to be reset. In that case, since no background estimates were available, an iterative and converging detection was implemented, providing also the initial values of the running estimates. Running estimates could fail in case of too few background samples being available, but such events were very rare.

6.5. Programme Star Detection by FAST

The Multi-Step Detection

The aim of this processing step was to detect in a star mapper record the signal, if present, of the programme star whose transits were expected to be sufficiently accurate for the attitude determination. So, the objective was to detect an isolated and unperturbed transit per record generated by the programme star—a transit of this kind was referred to as an attitude star transit. To meet this objective, an attitude star had to be detected not only with respect to the background, but very often among different star signals generated by overlapping parasitic or programme stars. This situation caused two main risks of not reaching the objective:

(1) the multiple star risk: the risk of detecting more than one candidate star without being able to select the expected programme star. In this case, a potentially useful transit might have to be rejected to the detriment of the attitude estimation process, in particular when few transits were available or when the attitude underwent quick variations. This risk could be reduced for the transits of bright stars by isolating in the record only sufficiently bright signals;

(2) the false transit risk: the risk of obtaining one isolated but false programme star detection and hence generating an erroneous transit time for the attitude reconstruction. This risk was particularly high in the records of faint programme stars, owing to the relatively large number of potential parasitic stars of similar magnitude. For those transits, it was preferable to increase the chance of detecting more stars, in order to accept more isolated programme stars.

Such a complex detection problem could not rely only on accepting or rejecting single samples of the convolution $T_0(m)$, but instead, it demanded a multi-step detection procedure applied to a suitable group of samples. The main steps are described below, further details are shown in the flow chart in Figure 6.10:

(1) detecting a star: any group m of four samples separated by the calibrated slit spacings d_j was tested for how many samples could be accepted as generated by the same star. Note that m indicates the sample corresponding to the fiducial reference line. The four convolutions $T_j(m)$, $j = 1 \ldots 4$ represented the four slits at the

distances d_j relative to the reference line for sample m. As already explained, each one was associated with a boolean variable $L_j(m)$ indicating whether the signal was above the given threshold s. By adapting the threshold to the star magnitude, the test was made more or less selective, according to the objectives assigned. The four variables $L_j(m)$ were added to produce the variable $H(m)$, having values from 0 to 4 according to the number of accepted samples. $H(m)$ was defined only when all $T_j(m)$ were defined, i.e. when all four slit responses were contained within the 200 samples record;

(2) detecting a single star: when m coincided with the transit time of a star, $H(m)$ was equal to 4. Some neighbouring values of $H(m)$ would also be equal to 4, in particular for a bright star. Thus, when a position $\hat{m}$ was found with $H(\hat{m}) = 4$, the neighbouring samples $\hat{m} + k$, $k = \ldots -1, 0, 1, \ldots$ were checked until $H(\hat{m} + k) < 3$. This set of samples, $\mathcal{S}(\hat{m})$, constituted the detection of a transit with provisional transit time equal to $t_{\hat{m}}$. When still other samples were detected with $H(m) = 4$, without being contiguous to $\mathcal{S}(\hat{m})$, the record was assumed to contain more than one transit and was rejected;

(3) detecting a single, unperturbed transit: transit signals could be perturbed by spikes or closely overlapping other transit signals, in a way that could not be detected in the preceding step. To discriminate unperturbed transit signals, suitable two step χ^2 tests were applied to the convolutions $T_j(\hat{m})$;

(4) detecting an attitude star transit: when only one transit was detected in the record, and this transit was accepted as single and unperturbed, the transit was accepted as the result of the attitude star transit and used for the attitude reconstruction process.

Some of these steps are now described in more detail.

Detecting a Stellar Transit

To detect a transit, the four tests $T_j(m) \geq s_1$ $(j = 1 \ldots 4)$ were applied to each sample group m, resulting in the boolean variables $L_j(m)$. The tests discriminated between two hypotheses H_s^* and $\mathrm{H}_0 \cup \mathrm{H}_p^*$, where H_s^* is the composite hypothesis that the sample is biased by a transit signal from a star as bright as or brighter than the expected programme star (the so-called candidate stars). For each transit record, the detection threshold was computed as:

$$s_1 = \max(s_0, T^*), \quad T^* = \bar{I}_b \int R_q(t)\mathrm{d}t + I_s \int R_q^2(t)\mathrm{d}t \qquad [6.9]$$

where s_0 is defined in Equation 6.6, T^* is the lower limit of the convolution average under hypothesis H_s^* and I_s the *a priori* estimate of the programme star intensity for channels B_T and V_T together. This threshold was designed to reduce the risk of accepting as a candidate transit a too faint, and hence probably parasitic, transit. At this stage, I_s was computed from the (uncertain) catalogue magnitude M and colour index $B - V$, with a safety margin applied to account for the uncertainty in these values:

$$M_0 = M + 0.5(B - V) + 0.5, \quad M_0 \leq M + 1.25 \qquad [6.10]$$

As the expected magnitude approached the highest programme magnitudes (9 to 10), the threshold s_1 was less and less effective in reducing the multiple star risk, in agreement with the objective of avoiding false transits. Since those magnitudes were comparable

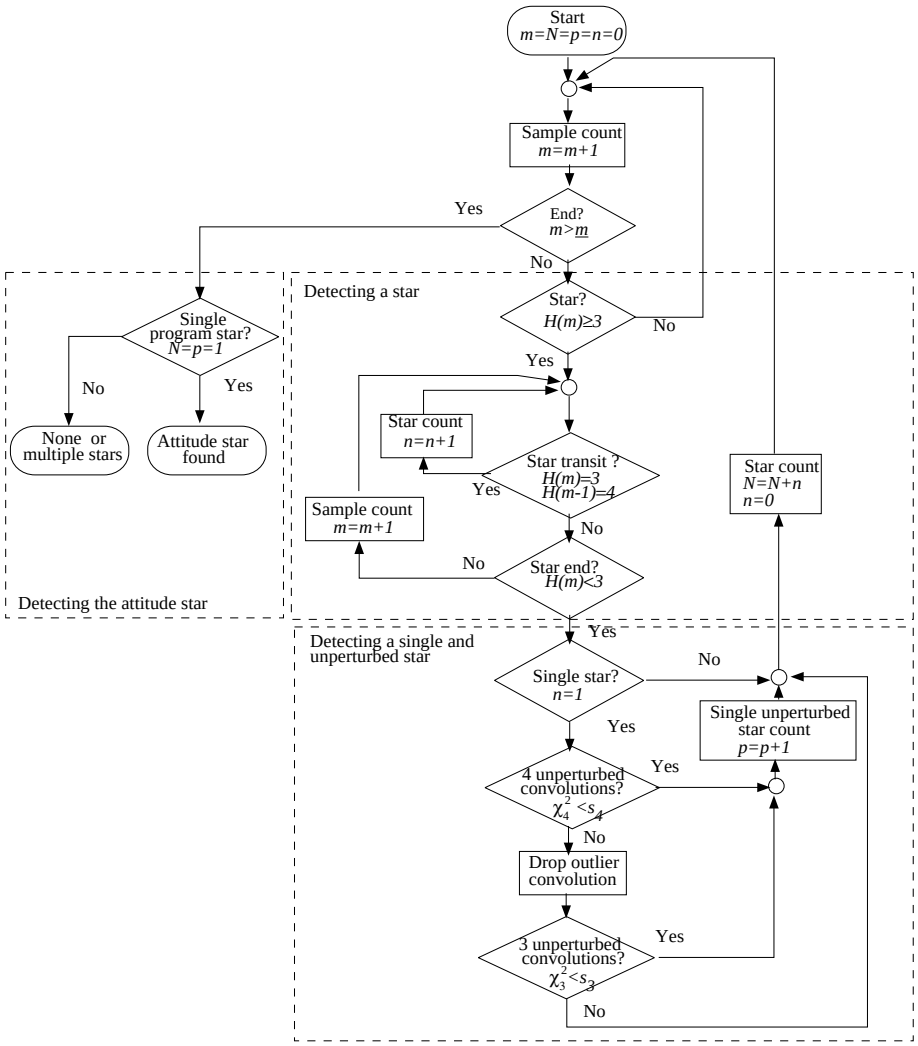

Figure 6.10. *Flow chart of the programme star detection.*

to background, the threshold s_1 had to be more effective in separating star samples from background samples and consequently was forced to be equal to s_0.

Perturbed Transits

Quite frequently a star-transit signal was partially perturbed by the transit of a brighter programme star or by unpredictable spikes. This could lead to an inaccurate transit time estimate. To reduce this risk, the following strategy was applied:

(1) the four convolutions $T_j(m)$ for a transit were tested through a χ^2 test, $\chi_4^2 \geq 16$, to detect outliers. When the test was significant, the higher outlier, e.g. the convolution $T_i(m)$ corresponding to photon-counts collected during the passage of slit i, was dropped from the subsequent processing. Otherwise the transit was accepted as unperturbed;

(2) the remaining three convolutions were tested again for $\chi_3^2 \geq 9$. When this test was significant too, the transit was rejected.

In the case of spikes outside the star signals, two risks had to be managed:

(1) the risk of accepting it as background—this was managed by the background detection process;

(2) the risk of accepting it as part of a star signal—this risk happened to be very low, as most spikes could only yield a test variable $H(m) = 1$.

First Transit Time and Intensity Estimates

When a single and unperturbed transit had been detected, a first estimate of the four transit times τ_j and of the stellar intensities I_{s,V_T} and I_{s,B_T} was obtained. The four samples $\hat{m}_j$ of the group $\hat{m}$ detected as the maximum of the test variable $H(m)$ in the set $\mathcal{S}(\hat{m})$ of the single transit, were taken as a first estimate of the slit transit times τ_j. All the peak samples around $\hat{m}_j$ were then used to provide the first estimate of the stellar intensities in both channels.

6.6. Transit Time and Intensity Determinations by NDAC

The estimation of the transit time τ and intensity I_s were linked in an iterative loop. All estimates were obtained through linear least-squares. In the first iteration step, equal weights were used. In subsequent iteration steps the weights were derived from the estimated values of the preceding preliminary solution. Effectively, this was equivalent to a joint maximum likelihood estimation of the two parameters.

Successive estimates of the transit time and its standard error were obtained from corrections to the previous values. The differences between the observed counts $N_{k,c}$ and a preliminary model fit, using the transit time $\tilde{\tau}$, were related to the required correction $\Delta\tau$ in the transit time estimate through the derivative of the single-slit response function, $R'_q = \mathrm{d}R_q(t)/\mathrm{d}t$ (see Figure 6.4). Excluding the noise term, Equation 6.1 gives:

$$N_{k,c} - I_{b,c} - I_{s,c} \sum_{j=1}^{4} R_q(t_k - \tilde{\tau} - d_j/v_q) = -I_{s,c} \sum_{j=1}^{4} R'_q(t_k - \tilde{\tau} - d_j/v_q)\Delta\tau \qquad [6.11]$$

Equation 6.1 was used for solving $I_{s,c}$ using estimated values of τ, while Equation 6.11 was used for obtaining corrections to $\tilde{\tau}$ using the estimated values for $I_{s,c}$. Estimating all the parameters at the same time proved hazardous due to disturbances of the star mapper signal. Spikes, possibly caused by cosmic rays, could not always be recognised before processing started, but were able to distort a solution with too many degrees of freedom. Thus, the above-described iterative approach was adopted. Solutions generally converged rapidly. Figures 6.11 and 6.12 show the astrometric and photometric precision reached with these reductions. Also shown in each case is the slope of a relation where the error is proportional to the photon noise on the signal. This does not apply to faint stars, where the relative error is larger due to the significant contribution of the background signal. From Figure 6.11 it is clear that the majority of star mapper transits

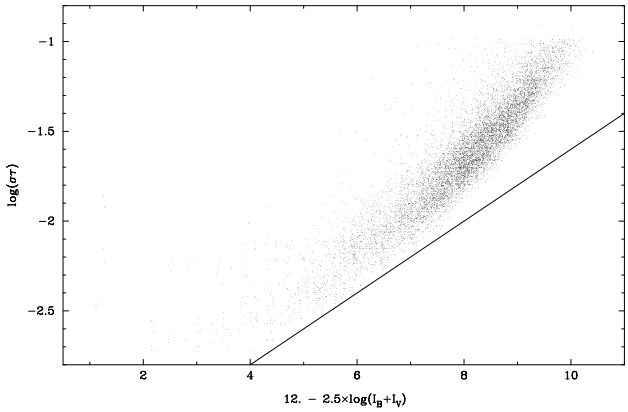

Figure 6.11. *The noise levels on the transit times (σ_τ, in arcsec) as a function of the total signal intensity. The graph shows the results for 9400 reduced star mapper transits obtained over a period of 9 hours in the beginning of 1990. The horizontal scale presents the observed counts as approximate magnitudes.*

contributing to the attitude reconstruction process had transit time errors between 0.1 and 0.01 arcsec.

The approach described above allowed for the solution of the parameters for more than one signal. This was used for double stars and for recovery of transits disturbed accidentally by another transit (usually from the other field of view). In the case of double stars the predicted separation was used to recognise the signal. Only double stars with separations larger than 1.5 arcsec were treated this way. As it was not known generally where an accidentally superimposed transit originated (which slit group, field of view, etc.,) the correction procedure was not ideal, being unable to implement the proper scan velocity and single-slit response functions for the stray transit.

6.7. Transit Time and Intensity Estimation by FAST

Transit Time Estimation

In principle, the first estimate $\hat{m}_j$ of the transit times provided by maximizing the photon count convolutions (Equation 6.5), and having the resolution of the samplings (0.28 arcsec), could have been refined by interpolating $T_j(m)$ around the maxima. Unfortunately, convolutions are not an acceptable approximation of the log-likelihood function (Equation 6.4) for this task, since they tend to the log-likelihood function only when $I_s/I_b \rightarrow 0$. Therefore a better approximation, still independent of the star intensity, was used, with the constraint of accurately approximating the log-likelihood function at least for the faintest programme stars, i.e. $I_s/I_b \simeq 1$. The new function can be shown to be the convolution of the photon-counts with $\ln[1 + I_s R_q(t)/I_b]$ (see also Perryman *et al.* 1989, Volume III, Chapter 3). Moreover, by imposing $I_s/I_b = 1$, the approximate likelihood function is made independent of star intensity and reads:

$$\ln L(\tau_j) = \sum_{c=B,V} \sum_{k} N_{k,c} \ln[1 + R_q(t_k - \tau_j)], \quad j = 1 \ldots 4 \qquad [6.12]$$

Maximizing this function with respect to τ_j, using a sufficient time resolution, provided efficient transit time estimates $\hat{\tau}_j$ for at least the faintest programme stars. Moreover, by quadratically interpolating $\ln L(\tau_j)$ around the maxima, the negative inverse of the second derivative (Hessian) could be computed, providing the variance of the transit time estimate.

A suitable χ^2 test, with a low risk (0.1 per cent) of the first kind, was then applied to the four estimated times $\hat{\tau}_j$ to detect any possible outlier which could arise due to partial overlapping by a parasitic transit. When the test was significant, the outlier was dropped from subsequent processing. The transit time τ across the fiducial reference line was then estimated from the model:

$$\hat{\tau}_j = \tau + d_j / v_q + \epsilon_j \qquad [6.13]$$

where the index j denotes the peaks of the transit signal accepted by the detection procedures (a minimum of three), and ϵ_j their estimation error. In the normal case of four accepted measures, the estimate of the transit time was given by:

$$\hat{\tau} = \frac{1}{4} \sum_{j=1}^{4} \hat{\tau}_j \qquad [6.14]$$

The residuals of the above estimation were calculated *a posteriori*, using accurate estimates of the scan velocities, to assess the accuracy of the transit time estimator. Under the assumption of a known scan velocity v_q, Equations 6.13 could be transformed by the following orthogonal matrix $\mathbf{T}$:

$$\mathbf{T} = \frac{1}{4} \begin{pmatrix} 1 & 1 & 1 & 1 \\ 1 & -1 & -1 & 1 \\ 1 & -1 & 1 & -1 \\ 1 & 1 & -1 & -1 \end{pmatrix} \qquad [6.15]$$

The first row of the transformed equation yielded the transit time estimate as in Equation 6.14; the other three rows yielded three uncorrelated residuals having the same variance as the transit time estimation. By collecting such residuals, the *a posteriori* standard deviation of the transit time was assessed.

Intensity Estimation

After the transit of an attitude star had been detected, and the transit time was estimated, the log-likelihood function (Equation 6.4) could be solved for the photometric parameters through the following gradient equations (one set for each channel c), applied to the sequence $\mathcal{C}$ of model-consistent photon counts:

$$\frac{\partial \ln L(I_{s,c}, I_{b,c})}{\partial I_{s,c}} = \sum_j \sum_{k \in \mathcal{C}} \frac{N_{k,c} - I_{k,c}}{I_{k,c}} R_q(t_k - \hat{\tau}_j) = 0 \qquad [6.16]$$

and:

$$\frac{\partial \ln L(I_{s,c}, I_{b,c})}{\partial I_{b,c}} = \sum_{k \in \mathcal{C}} \frac{N_{k,c} - I_{k,c}}{I_{k,c}} = 0 \qquad [6.17]$$

Since the above equations are not linear in the unknown parameters, they would have required an iterative solution. In practice, a single-step solution was used, after obtaining estimates for the weight $w_{k,c} = 1/I_{k,c}$ from the available background estimates and the first estimates of the star intensities provided by the detection step. This simplified

procedure corresponds to the weighted least-squares solution of the following linear equations:

$$N_{k,c} = I_{b,c} + I_{s,c} \sum_j R_q(t_k - \hat{\tau}_j) + \epsilon_{k,c}, \quad \mathrm{Var}(\epsilon_{k,c}) = I_{k,c} \qquad [6.18]$$

which proved to be accurate enough for the photometric parameters.

6.8. Comparisons

Several comparison exercises were carried out in the beginning of 1991 at the Royal Greenwich Observatory, involving star mapper reduction results obtained by NDAC, FAST (main processing and 'First Look') and TDAC. At that stage there was very good consistency with transit time and intensity determinations. Since then, some changes have taken place in the software, most notably by FAST. No direct comparisons were done with results obtained after implementation of those changes, although indirectly the star mapper transit time results were checked in the attitude reconstruction comparisons, described in Chapter 7.

6.9. Star Mapper Astrometry

The reduced star mapper data in combination with the reconstructed attitude contained positional information for the observed stars. The standard errors of the positions provided by the Hipparcos Input Catalogue were 3 to 6 times larger than the possible standard error of the attitude fit. As a result, the differences between the predicted positions (based on the Input Catalogue) and the observed positions (based on the transit times and the reconstructed attitude) represented at least partially the positional errors that were present in the Input Catalogue.

In the NDAC data reductions these differences were accumulated in a 'working catalogue', containing next to *a priori* data several small information arrays, representing least-squares solutions of positional and magnitude corrections. These were updated using a Householder transformations based mechanism every time new data became available, and could be solved for the updates at any time. During the first 18 months of the mission this information was used to improve the stellar positions used by the satellite for its real-time attitude determination, leading to a considerable improvement in performance.

6.10. Star Mapper Photometry

The star mapper intensity estimates were used to derive the B_T and V_T magnitudes, which were used during the mission to improve the colour information made available through the Input Catalogue (which was in many cases only an estimated value). The intensities were calibrated with respect to a set of standard stars constructed for the Tycho photometric reductions.

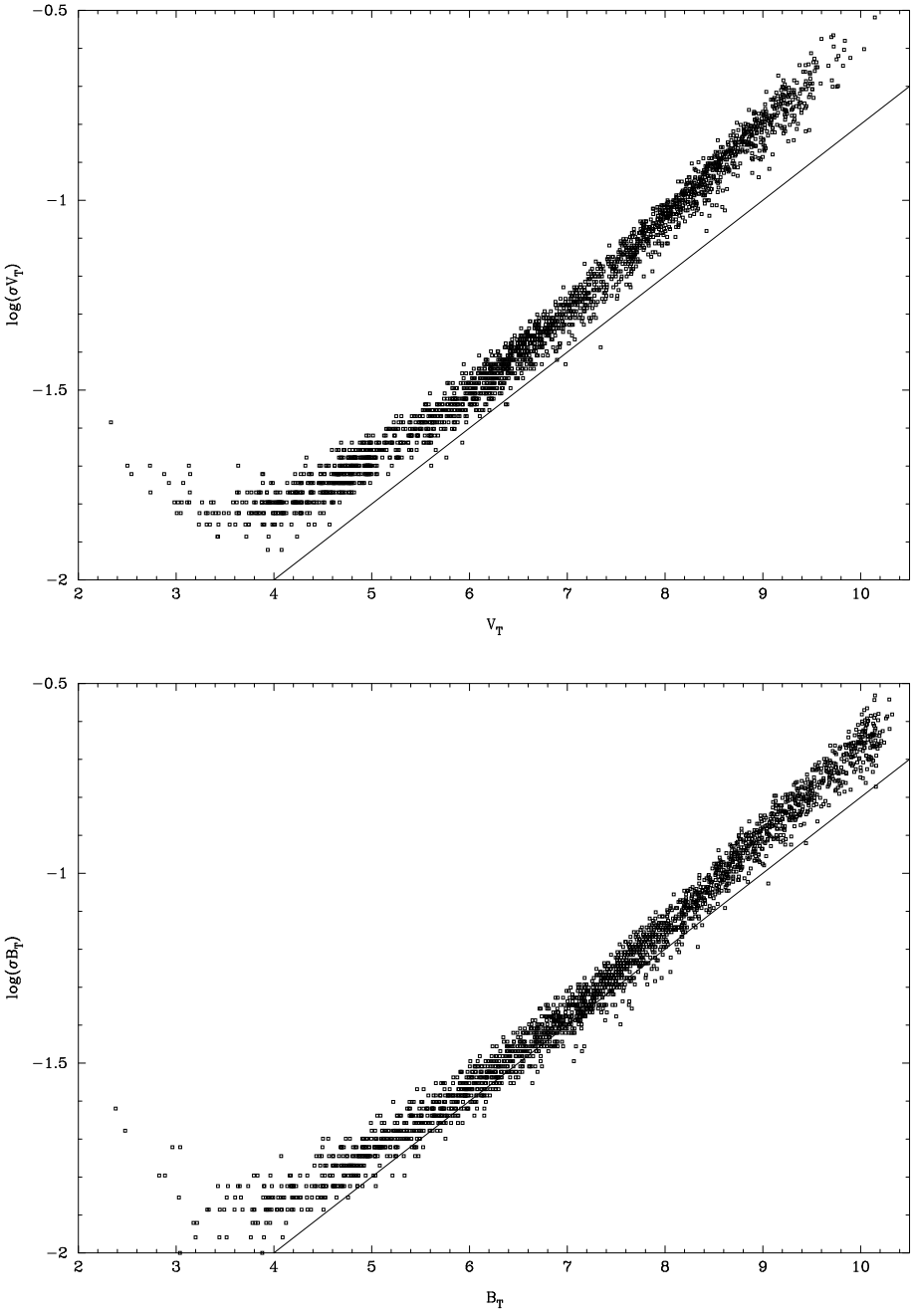

Figure 6.12. *The noise levels on the accumulated V_T and B_T magnitudes for constant stars.*

The calibrations were carried out in relative intensity scale. The magnitudes of the calibration stars were converted to a pseudo intensity by:

$$I_c = 10^{-0.4(M-10)} \qquad [6.19]$$

where $M = B_T$ or V_T was the magnitude of the calibration star. The calibration used the following model:

$$I_s/I_c = a_1 + a_2 C + a_3 C^2 + a_4 z + a_5 z^2 + a_6 C z \qquad [6.20]$$

where $C = (B_T - V_T) - 0.7$ stands for the colour of the star, and a_i are the unknown parameters. z is the vertical coordinate of the transit. Calibrations were done over data accumulated for an average of 2 to 3 days. They were done separately for the inclined and vertical slit groups, preceding and following fields of view and for the B_T and V_T channels, giving 8 calibrations in total. The star mapper detectors were much less affected than the image dissector tube detector by transmission loss due to radiation. This meant that longer stretches of data could be used in the reductions.

A 'running solution' was used, where the solution obtained for the preceding data interval was used as additional, down-weighted, observation equations, again using a Householder transformations based least-squares routine.

As the effective integration time for a star mapper signal was fixed, the errors on the individual photometric measurements were proportional to the inverse of the square root of the intensity. This is evident in Figure 6.12, where the $\log(\sigma_M)$ is plotted against magnitude, showing also the expected relationship. The increase in errors for faint magnitudes is due to background contributions, on the bright end due to modelling inaccuracies. The errors on the mean magnitudes are on average a factor 10 smaller. Variable stars were excluded from the diagrams.

The response in the star mapper channels decreased by an average of 3 per cent per year, a total of about 12 per cent over the mission (see also Volume 2, Figure 10.2). This compares with a decrease of around 40 per cent in the image dissector tube detector (see Chapter 14). The response in the vertical slits was sensitive to focus variations.

More details on star mapper photometry can be found in Volume 4, Chapter 8.

F. van Leeuwen, E. Canuto, F. Donati, J. Kovalevsky